LA-13227

KISMET Tungsten Dispersal Experiment

Los Alamos
NATIONAL LABORATORY

Los Alamos National Laboratory is operated by the University of California for the United States Department of Energy under contract W-7405-ENG-36.

An Affirmative Action/Equal Opportunity Employer

LA-13227

UC-700
Issued: December 1996

KISMET Tungsten Dispersal Experiment

Kenneth Wohletz
Thomas Kunkle
Ward Hawkins

Los Alamos
NATIONAL LABORATORY
Los Alamos, New Mexico 87545

KISMET Tungsten Dispersal Experiment

Kenneth Wohletz, Thomas Kunkle, and Ward Hawkins

ABSTRACT

Results of the KISMET tungsten dispersal experiment indicate a relatively small degree of wall-rock contamination caused by this underground explosive experiment. Designed as an add-on to the KISMET test, which was performed in the U-1a.02 drift of the LYNER facility at Nevada Test Site on 1 March 1995, this experiment involved recovery and analysis of wall-rock samples affected by the high-explosive test. The chemical, high-explosive blast drove tungsten powder, placed around the test package as a plutonium analog, into the surrounding wall-rock alluvium. Sample analyses by an analytical digital electron microscope (ADEM) show tungsten dispersed in the rock as tiny (<10 μm) particles, agglomerates, and coatings on alluvial clasts. Tungsten concentrations, measured by energy dispersive spectral analysis on the ADEM, indicate penetration depths less than 0.1 m and maximum concentrations of 1.5 wt % in the alluvium.

I. INTRODUCTION

Underground explosive testing requires some understanding of the dispersion of test materials into the host rock in order to evaluate the potential contaminant migration from the test area. In general, this information can be obtained by drill-back operations that recover samples of the rock adjacent to the test. But for mine-back reentry into the test area, knowledge of the potential range of hazardous material penetration around the test chamber (room) is important for human safety. This potential range is also useful for calculating posttest contaminant migration.

Small-scale underground explosive testing can involve test packages containing materials of potential concern for human safety. The KISMET experiment of 1995 (Kunkle, 1994) involved use of depleted uranium. In order to understand how plutonium might behave in a similar test, we used tungsten as a plutonium analog. With the objective of measuring how far tungsten would be embedded into the alluvium wall rock in the LYNER facility, we placed one kg of tungsten powder into three trays positioned on top and on the left- and right-rib sides of the explosive package.

The following report describes the method for sampling and analysis of the dispersed tungsten in the KISMET experiment (Kunkle, 1994) and results of tungsten concentration measurements in the samples of the LYNER facility alluvium. A first of its kind, this tungsten experiment is limited by the lack of knowledge about the physical behavior of the tungsten powder during the test, how it might interact with and penetrate the wall rock, and the amounts required to create measurable concentration profiles in the alluvium.

II. METHOD

One kilogram of commercially supplied tungsten powder (0.8 μm spheres) was placed into three trays, one on top of the explosive and one tray each on the left rib and right rib sides of the explosive. The test room was approximately a box shape, 3 m (10 ft) high and 3.7 m (12 ft) long and wide. The room floor (*invert*) was made of poured concrete, and the front of the room was defined by the inside wall of a massive concrete plug. The remaining four faces were native alluvium. This test room configuration provided ~72 m^2 (770 ft^2) of surface area of which ~46 m^2 (500 ft^2) was exposed alluvium.

Four of the five recognized rock types of the LYNER facility alluvium exist in the walls of the test room (Allen, 1995a). The alluvium consists of moderately to poorly sorted sands and gravels derived from a mixture of Tertiary volcanic and pre-Tertiary sedimentary and metasedimentary rock fragments. The units, described in Table 1, are mostly consolidated and are distinguished by the grain-size distribution of their clasts.

Table 1. Map unit (bed type) classification of U-1a.01 LYNER facility*

Map Unit (bed type)	*Cobbles %*	*Pebbles %*	*Sand %*	*Silt %*	*Clay %*
Type 1: sand bed	0-1	6-19	64-85	4-16	1-4
Type 2: sandy pebble bed	0-5	10-50	46-72	3-9	0-3
Type 3: pebbly cobbly sand bed	5-20	10-30	42-65	2-11	1-6
Type 4: cobbly sandy pebble bed	0-10	25-54	36-62	3-5	1-2
Type 5: cobble bed	25-40	10-30	40-60	8-9	2-3

**The KISMET test room exposed map units 1 through 4, of which only 1, 2, and 4 were sampled. The relative average clast size of these units is 1 < 4 < 2 < 3 < 5.*

The method used to evaluate the dispersion of tungsten involved: (1) recovery of rock samples from the ribs, face, and back of the KISMET zero room; (2) preparation of thin sections of the samples for imaging in an analytical digital electron microscope (ADEM); and (3) measurement of tungsten concentrations within the samples by energy dispersive spectral (EDS) analysis of x-rays emitted from the samples during their exposure to a 20 keV beam in the ADEM.

The KISMET reentry sampling (Allen, 1995b) was conducted on April 18-19, 1995. We designed the procedure to recover tungsten embedded in rocks of the zero room walls to evaluate areal dispersion patterns, depth of penetration, and sensitivity to rock lithology. In order to achieve samples representing variability in tungsten concentration with spatial distribution,

lithological variation, and depth of penetration, we chose 0.3- to 0.6-m^2 sample locations on the ribs, face, and back of the zero room, which we demarked by orange spray paint: three each on the left and right ribs, 6 on the face, and one area on the back (Figs. 1 to 3). For each area we chiseled samples out of the wall over three depth intervals to a depth of ~0.01 m. We also obtained surface samples for each location by scraping soot and loose dust that generally covered most of the walls. To preserve the initial orientation of bulk intact samples, we painted the outer surfaces of each sample. Where the wall rock crumbled during sampling, such that intact samples could not be taken, we chiseled fragmental samples from the measured depth interval. The zero room alluvium included 4 lithological types, and the sample lithology is noted on maps of the ribs and face of the zero room (Figs. 1 to 3).

To establish the physical character (solid particles, congealed melt) and distribution of the tungsten, samples were analyzed with an analytical digital electron microscope (ADEM). For this analysis, samples were prepared by making thin sections. For intact, oriented samples, polished, 30-μm-thick slices of the rock were cut and epoxied onto glass slides with sample orientations scribed on the slides. Particulate samples were impregnated with epoxy, cut (30 μm thick), mounted onto glass slides, and polished. The ADEM was operated in scanning electron microscope (SEM) mode using backscattered electrons to image the sample at various magnifications. Backscattered electrons produce images whose brightness and contrast are sensitive to atomic weight, such that heavy metals such as iron (typically present in samples of alluvium) and tungsten are readily distinguished. Compositions of selected areas of various sizes were achieved by measuring the energy of x-rays emitted from the sample under the electron beam. A 20-keV-beam potential was used to stimulate x-rays representative of all major fluorescence modes of tungsten.

For analysis, the M-α x-rays of tungsten overlap those of silicon, which is very abundant in all samples, so L-α x-rays were counted to measure tungsten. Because a standard for tungsten embedded in alluvium does not exist, a standardless method, based on Z-number, absorbance, and fluorescence (ZAF), was applied. This method gives semiquantitative results as stoichiometric weight percents. These results however, are adequate for evaluating the relative concentrations of tungsten among samples. In addition, where oriented samples were analyzed and a tungsten concentration variation with depth was expected, line scans were performed. The line scans show the variation of tungsten L-α x-ray emission along a profile. These profiles are quantified only by the number of x-ray counts per second.

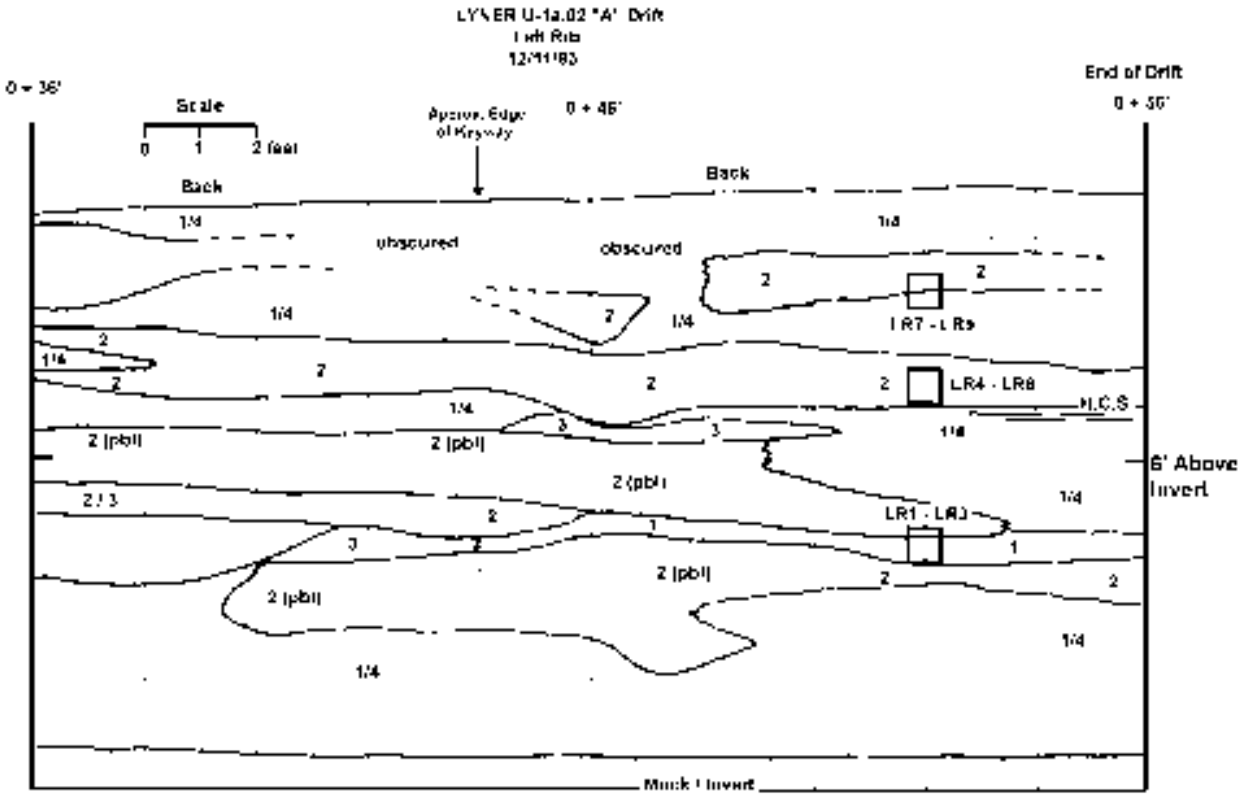

Figure 1. Geologic map of the U-1a.02 drift left rib, modified from Allen (1995a). Map units (Table 1) are numbered [2 (pbl) refers to unit 2 with pebbles, H.C.S. refers to high concentration of sand, and numbers separated by a slash designate mixed lithologies]. Sample locations are shown in boxed areas with sample numbers.

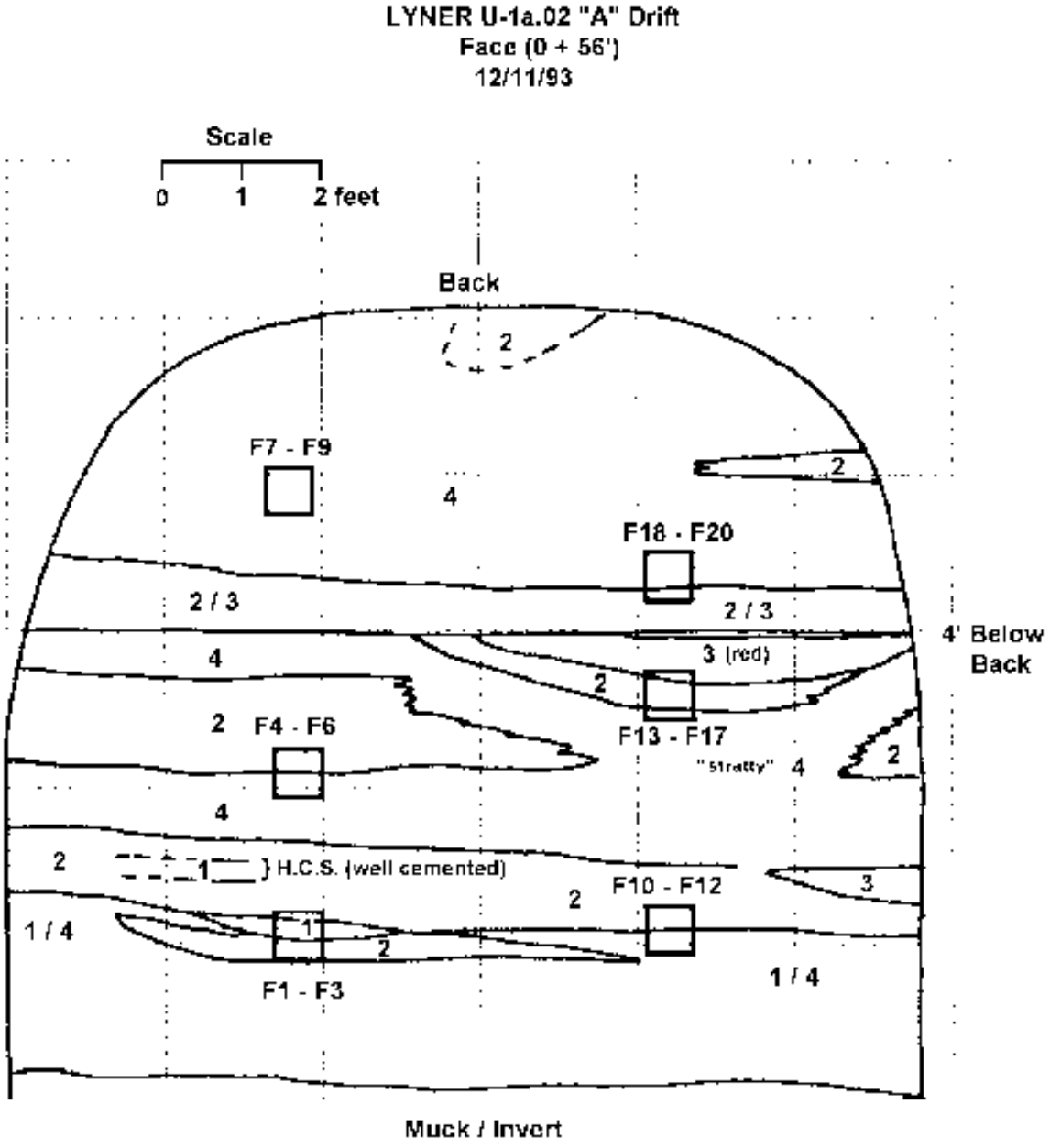

Figure 2. Geologic map of the U-1a.02 drift face, modified from Allen (1995a). Map units (Table 1) are numbered ("stratty" refers to bedded), and sample locations are shown in boxed areas with sample numbers.

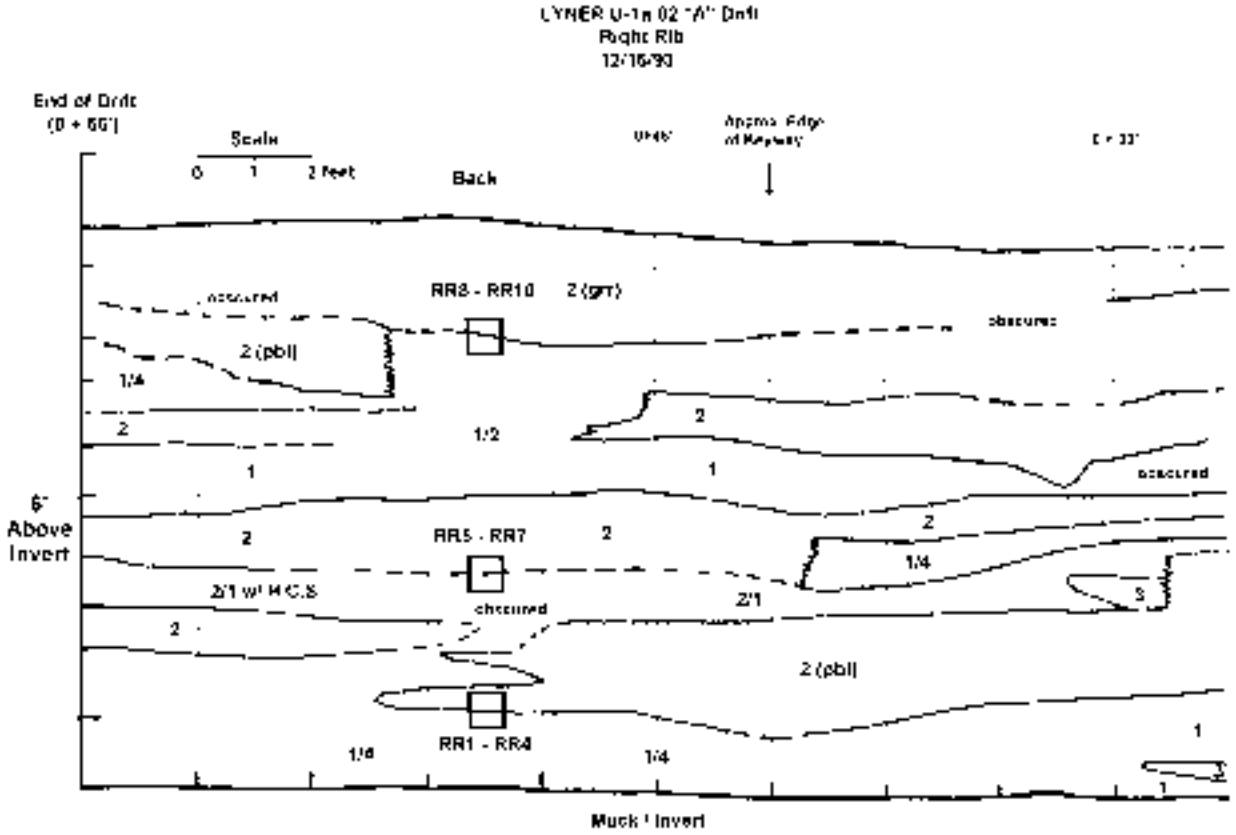

Figure 3. Geologic map of the U-1a.02 drift right rib, modified from Allen (1995a). Map units (Table 1) are numbered [2 (grr) refers to unit 2 with gravel], and sample locations are shown in boxed areas with sample numbers.

III. RESULTS

Tungsten occurs as very heterogeneously dispersed agglomerated masses, coatings, and small spherical particles. Its most common form is particles mixed into microvesicular agglomerates of quenched iron. In Figure 4, an SEM microphotograph taken from backscattered electrons, bright areas correspond to high Z-number particles composed of iron and tungsten mixtures (the tungsten areas are brightest). Most of these mixed particles have vesicles, which likely formed from gases trapped in the rapidly congealed iron, melted by the blast. Tungsten can also occur as individual spherical particles, but as shown in Figure 5 these are only easily viewed where they have agglomerated into masses generally <10 μm in diameter. Some of these tungsten particles are agglomerated into larger masses (Figure 6). Most distinctive are coatings of tungsten on small particles, illustrated in Figure 7. Generally these coatings are less than a few micrometers thick, but because of their brightness in backscattered images, they are readily visible in SEM views.

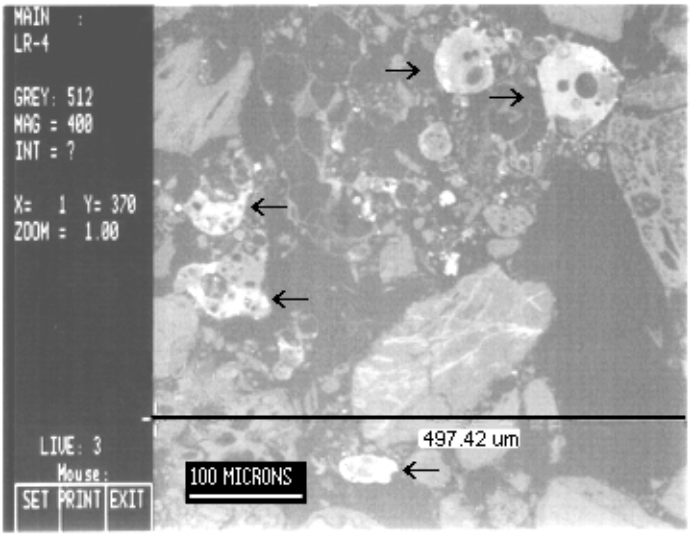

Figure 4. Example 0.5 x 0.5 mm (0.25 mm^2) area analyzed for tungsten in sample LR-4 (analysis 5). Note the 100-µm scale bar and the total width of the analyzed area (497 µm). Tungsten occurs as mixed patches (bright areas with arrows) in larger vesicular iron globules in this sample. The analysis of this area showed 2.78 wt % tungsten.

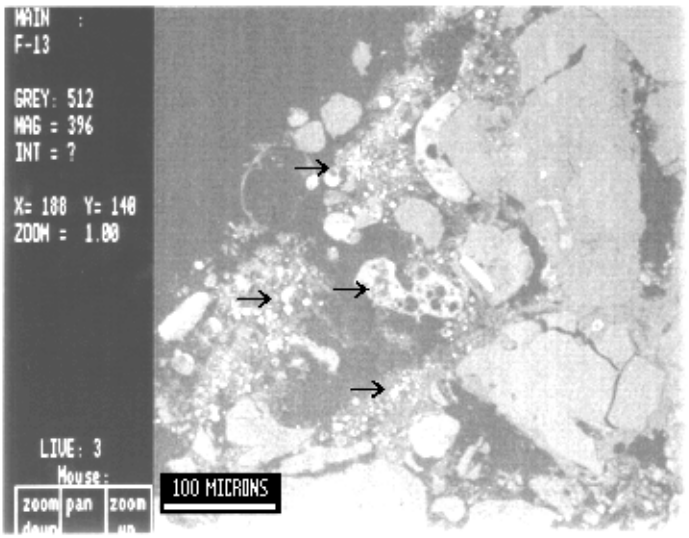

Figure 5. Example 0.5 x 0.5 mm (0.25 mm^2) area analyzed for tungsten in sample F-13 (analysis 8). Most tungsten occurs as tiny (<10 µm) particles (see arrows) that are generally stuck together or mixed in with larger vesicular iron globules. The analysis of this area showed 1.87 wt % tungsten.

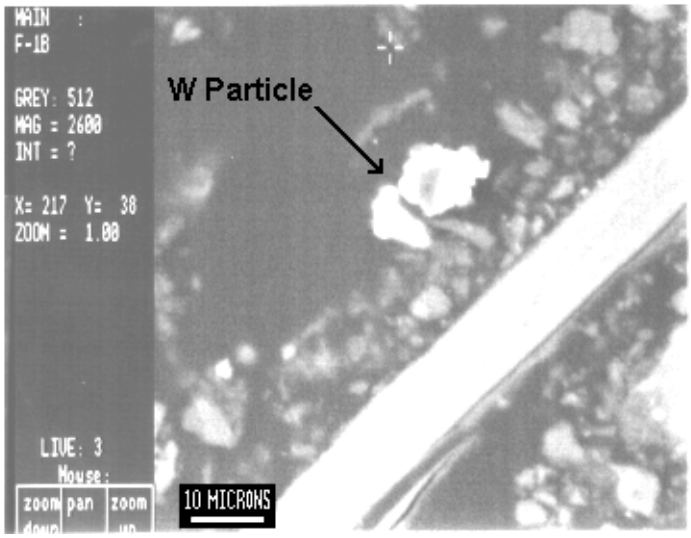

Figure 6. Close-up of tungsten particles (bright area) ~10 μm in diameter. Note that these two particles are actually combinations of numerous smaller particles stuck together.

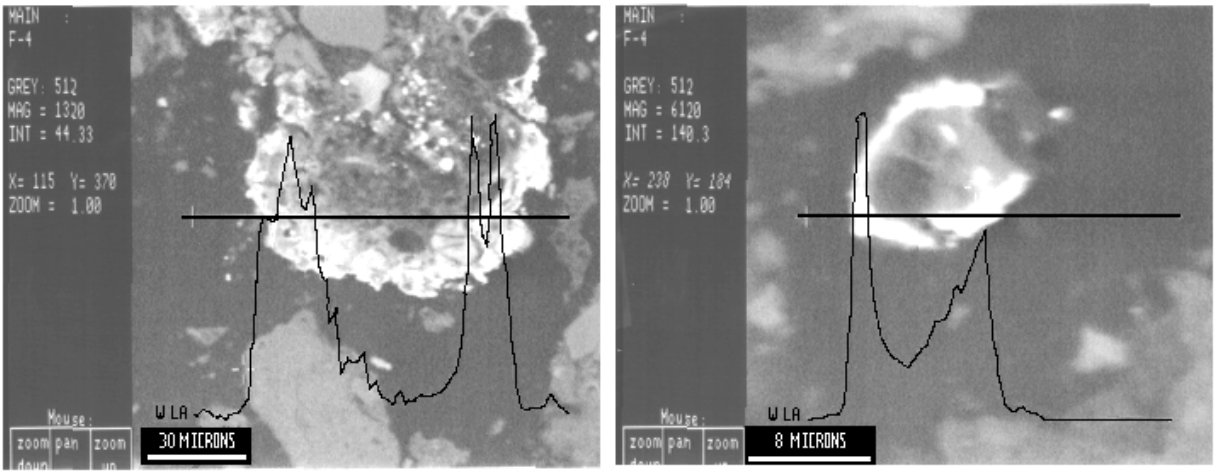

Figure 7. Two SEM microphotographs show tungsten coatings (bright areas) on large particles. Scans for tungsten L-α x-rays show peaks corresponding to where the scan crosses the tungsten encrustations.

Using the ADEM method described above, bulk area analyses covering >1 mm^2 generally did not show measurable tungsten. This finding is attributed to the fact that tungsten is extremely heterogeneously dispersed in samples, and where it exists, it is in the form of particles mostly less than 10 μm in diameter or as coatings on silt clasts of a similar size. For these reasons, analytical areas of 0.25 mm^2 were typically required to find measurable amounts of tungsten. In order to obtain analyses representing average tungsten concentrations for each sample, analyses were repeated over 10 separate areas and then averaged for each sample.

Table 2 lists average results for major chemical constituents in several samples representative of the lithologic variations of the KISMET test room alluvium. Since many of the sample areas included portions of several lithologic types, the relative abundance of each bed type is shown for each sample in Table 2. There are no other more precise major-element analyses available by which to check the results in Table 2, but considering the weathering likely to have occurred in the alluvium, these results are generally similar to intermediate volcanic rock compositions expected to be represented in the LYNER alluvium for the Nevada Test Site (Broxton et al., 1989; Warren et al., 1996).

Table 2. Representative Bulk Sample Analyses*

Constituent	***LR-2 1 >> 2***	***LR-8 2 = 1/4***	***F-2 1 = 2***	***F-6 2 = 4***	***F-7 4***	***LR-4 2***
Na_2O	0.63	0.60	0.79	0.35	0.40	0.44
MgO	0.68	0.31	0.56	0.74	0.66	0.54
Al_2O_3	13.02	10.21	10.39	13.01	13.17	11.75
SiO_2	57.78	54.95	60.98	57.15	57.55	59.84
K_2O	6.69	6.91	7.94	8.35	7.42	8.94
CaO	11.91	20.52	11.67	9.84	9.49	9.21
TiO_2	0.88	0.84	0.96	1.11	1.59	0.93
FeO_x	7.17	5.50	6.29	9.41	9.01	7.81
WO_x	0.38	0.18	0.00	0.04	0.73	0.54

**Analyses given in wt %; sample numbers and relative lithologic type (see Table 1 and Figures 1 to 3) are denoted for column headers. Fe and W oxides are listed as totals for their possible oxidation states (e.g., FeO_x = FeO + $FeO_{1.5}$, and WO_x = WO_4).*

In many samples tungsten particles were difficult to recognize, and many individual analyses found none. For each sample, the entire thin-section area was scanned to find areas likely to show tungsten, and these areas were preferentially analyzed such that the results obtained should represent maximum tungsten concentrations. For samples that were recovered intact and oriented, simple line scans for tungsten were expected to show gradients that decreased from the test room surface inward. Figure 8 illustrates a typical result for such a line scan of sample B-2, an intact sample of the alluvium extending from the surface of the back inward ~5 mm. Smooth concentration gradients were not found, owing to the particulate nature of the embedded tungsten. A general decrease with depth into the sample was only crudely demonstrated.

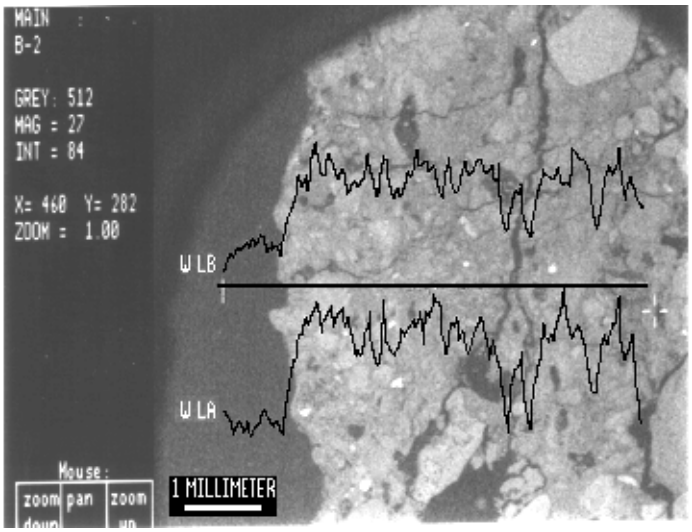

Figure 8. SEM photomicrograph of sample B-2, an oriented sample with the left edge at the surface of the KISMET test room alluvium extending inward to a depth of about 5 mm. The horizontal line shows the scan trace for tungsten L-α (W LA, plotted below the line) and L-β (W LB, plotted above the line) concentrations. Both concentration curves abruptly rise where the scan line crosses over the left edge of the sample and show only a crude decreasing trend in abundance with depth into the sample.

Table 3 shows averaged results for all the KISMET samples arranged into three groups: surface, near-surface, and deep sample analyses. Surface samples generally consisted of those obtained by scraping the outer 1 mm of the alluvium, which generally included the thin film of soot from the blast. The results for these surface samples (0 to 1 mm deep) center fairly consistently around an average concentration of 0.77 wt % tungsten. Near-surface samples (representing the outer 32 mm of the alluvium) averaged around 0.24 wt %, whereas deep samples (~25 to 64 mm deep) averaged only 0.11 wt % tungsten. These results support the hypothesis that tungsten concentration decreases with depth into the alluvium.

To further investigate the distribution of tungsten, simple histograms were prepared, depicting the concentration of tungsten as a function of sample depth, lithology, and location. Figure 9 shows the generally decreasing tungsten concentration observed for samples taken from increasing sample depth. There are notably high values at 13, 38, and 64 mm depths, a result discussed below. Tungsten concentrations also show a crude increase in alluvial lithologies of coarser grain size (Figure 10). Because the explosive apparatus with the tungsten was placed closer to the drift's left rib and face, the greater abundance in those positions shown in Figure 11 is expected. Below we analyze these results to derive a predictive model for tungsten distribution for the KISMET test.

Table 3. Tungsten Analysis Results

Sample Number*	***Sample Lithology**†*	***Depth (mm)***	***Tungsten (wt %)**††*	***Comments***
Surface				
LR-1	1 >> 2	0-1.0	0.000	loose surface soot
LR-2	1 >> 2	0-0.5	0.654	--
LR-4	2	0-1.0	0.580	loose surface soot
LR-7	2 = 1/4	0-1.0	0.541	loose surface soot
F-1	1 = 2	0-1.0	0.446	mostly loose surface soot
F-5	2 = 4	0-1.0	0.694	mostly loose surface soot
F-7	4	0-1.0	0.728	little/no soot
F-10	2 = 1/4	0-1.0	0.739	mostly loose surface soot
F-13	2 >> 3 + 4	0-0.5	1.119	oriented, intact, edge
F-14	2 >> 3 + 4	0-1.0	1.562	--
F-18	4 >> 2/3	0-1.0	1.010	gravelly lithology
RR-1	2 = 1/4	0-1.0	1.090	--
RR-5	2 = 2/1	0-1.0	0.716	mostly unconsolidated
B-1	2	0-1.0	0.980	mostly loose surface soot
Near Surface				
LR-5	2	0-25	0.684	mostly unconsolidated
F-19	4 >> 2/3	0-25	0.075	gravelly lithology
F-8	4	0-38	0.000	--
RR-6	4	0-38	0.034	mostly unconsolidated
RR-8	2 = 1/2	0-6	0.072	no soot (spalled surface?)
B-2	2	0-51	0.215	mostly unconsolidated
B-3	2	0-38	0.034	mostly unconsolidated
LR-8	2 = 1/4	0-38	0.175	oriented, intact
LR-2	1 >> 2	0-25	0.000	oriented, intact
F-2	1 = 2	0-25	0.000	oriented, intact
F-4	2 = 4	0-64	0.293	oriented, intact
F-6	2 = 4	0-64	0.039	oriented, intact
F-11	2 = 1/4	0-25	1.383	oriented, intact
F-13	2 >> 3 + 4	0.5-2.5	0.591	oriented, intact
F-15	2 >> 3 + 4	0-38	0.000	oriented, intact
RR-2	2 = 1/4	0-25	0.000	oriented, intact
RR-9	2 = 1/2	0-38	0.166	oriented, intact
FC-1	--	0-32	--	sample contaminated

Table 3. (Continued)

*Sample Number**	*Sample Lithology*†	*Depth (mm)*	*Tungsten (wt %)*††	*Comments*
Deep				
LR-3	1 >> 2	25-76	0.000	unconsolidated
LR-6	2	25-51	0.401	mostly unconsolidated
LR-9	2 = 1/4	38-76	0.139	intact pieces and dust
F-3	1 = 2	51-64	0.000	intact pieces and dust
F-9	4	51-64	0.000	--
F-12	2 = 1/4	38-51	0.082	oriented, intact
F-17	2 >> 3 + 4	38-51	0.000	--
F-20	4 >> 2/3	25-64	0.312	gravelly lithology
RR-3	2 = 1/4	25-64	0.050	oriented, intact
RR-4	2 = 1/4	64-89	0.000	intact pieces and dust
RR-7	2 = 2/1	38-89	0.209	mostly unconsolidated
RR-10	2 = 1/2	6-38	0.261	intact pieces and dust
B-4	2	38-64	0.000	mostly unconsolidated

**Sample numbers are designated by LR (left rib, Fig. 1), F (face, Fig. 2), and RR (right rib, Fig. 3).*
†Sample lithology is denoted by lithologic unit number and relative abundance. A slash between two numbers indicates a mixed lithology type.
††Tungsten concentration expressed as an average of 10 or more analyses of areas of 0.25 mm^2.

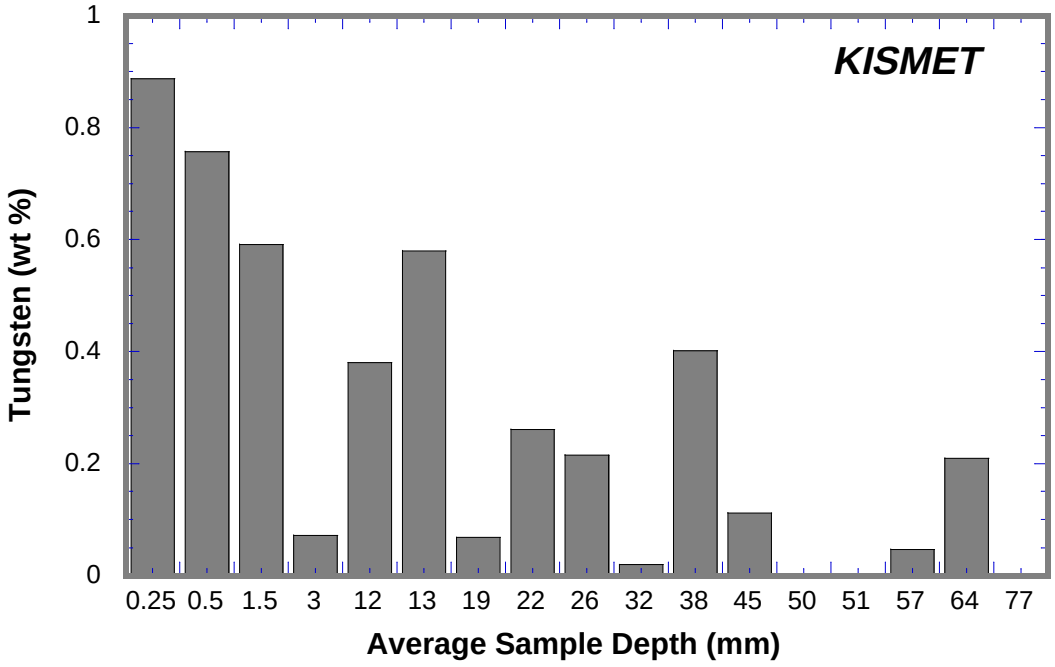

Figure 9. Average tungsten concentrations shown for samples taken from increasing depth in the LYNER facility alluvium. Because of the great variability of tungsten occurrence (many samples did not show tungsten), these averages have a standard error of about 50%.

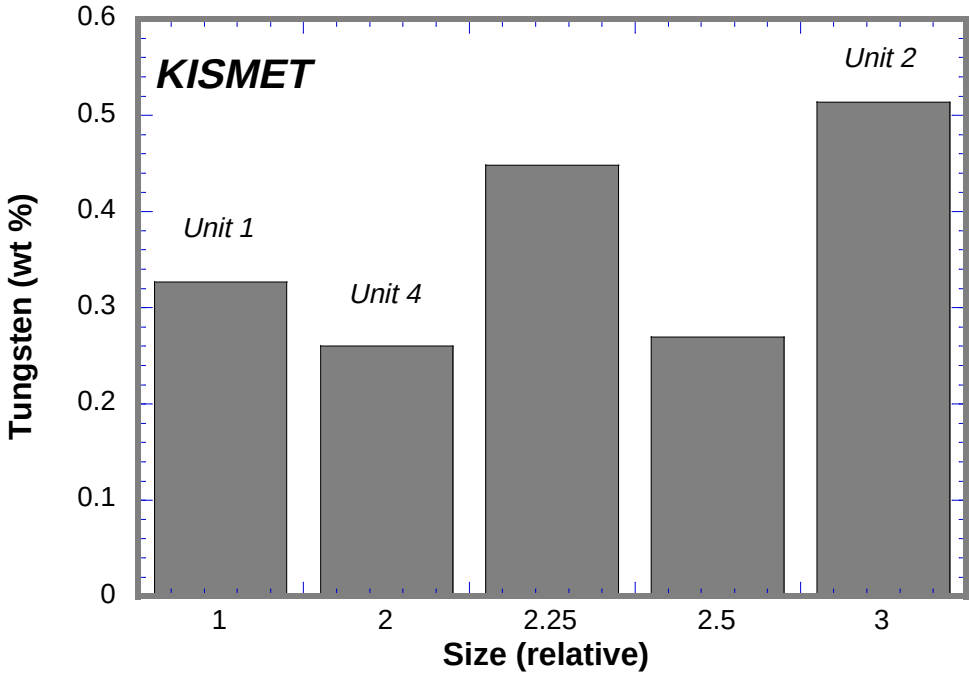

Figure 10. Average tungsten concentration for sampled map unit (lithologies) where map units have relative average clast sizes. Samples represented by relative size = 2.25 and 2.5 are combinations of map unit lithologies 1, 2, and 4. Map unit 3 was not sampled. Large error (100% of average value) for these average values exists because many samples showed little or no tungsten.

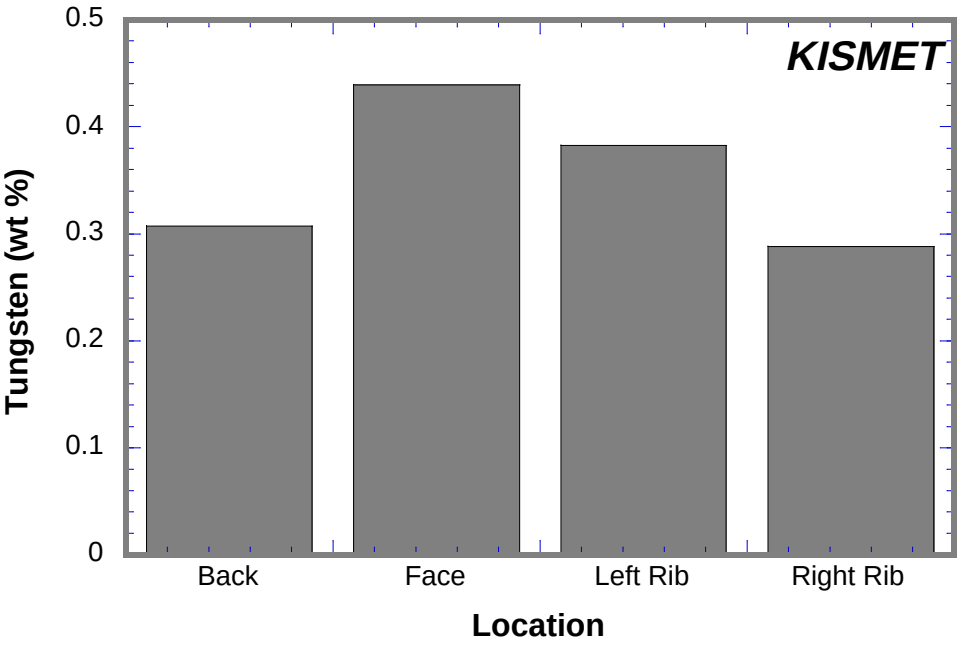

Figure 11. Average tungsten concentration for sampled locations. Standard error for these averages is about 100% of the average, as noted in Figure 10, because many samples showed little or no tungsten.

IV. DISCUSSION

If one assumes that the distribution of tungsten into the alluvium is driven by seepage of gas in the test room across fractured rock, the process can be described—through a simplification of the experimental geometry—as nonstationary, spherically symmetric filtration. Such a process may be analyzed (Adushkin and Spivak, 1994) by equations for conservation of mass and two-term filtration respectively:

$$\phi \frac{\partial \rho}{\partial t} + \nabla \cdot (\rho v) = 0 \quad , \tag{1}$$

$$\nabla p = -\frac{\mu}{k_1} v_f - \frac{\rho}{k_2} v_f^2 \sin v_f \quad . \tag{2}$$

In these equations ϕ is porosity, ρ is the gas density, t is time, v is the gas velocity, p is gas pressure, μ is gas viscosity, k_1 is the medium permeability coefficient, k_2 is the second permeability coefficient (often referred to as the *turbulence parameter* of the medium), and v_f is the filtration rate. As discussed by Adushkin and Spivak (1994), rock permeability can be idealized for a bed of spherical particles, a capillary model, a parallel jointed medium, or a serial model involving tortuous capillaries. To simplify the above considerations, if gas heat transfer and phase change are assumed negligible, the condition at the test room boundary is

$$\frac{\partial \rho}{\partial t} = -(\rho v) \frac{S}{V} \quad , \tag{3}$$

where S and V are the surface area and volume of the test room respectively. Nondimensional solutions of the above equation set by Adushkin et al. (1994) show filtration gas pressure and flow rate to exponentially decrease with time after the explosion and distance into the wall rock. Figure 9 suggests such a relationship with depth, assuming that tungsten concentrations are proportional to filtration rate and pressure.

Following the above suggestion that surface area and volume of the test room are important in determining boundary conditions for filtration, we offer the following analysis. First, assume that just after the explosion all of the tungsten was initially homogeneously dispersed in a gas (steam at 0.7 MPa, 800° C, density = 1.4 kg/m^3). If this gas uniformly filled the test room (40.8 m^3), then the alluvium was subjected to a source concentration of tungsten of ~1.73 wt %. If, however, all the tungsten dust was driven onto the surfaces of wall rocks (~71 m^2) by the blast, a maximum areal density of tungsten ~1.4 x 10^{-2} kg/m^2 might have characterized the initial moments of the test. If all this tungsten was embedded in the outer 0.5 mm of the walls (a rough measure of the average diameter of grains in the alluvium—a *medium sand*), then for an average alluvium density of 2600 kg/m^3 and average porosity of 35%, bulk concentrations of tungsten should average about 1.4 x 10^{-2} kg/0.85 kg rock (~1.6 wt %), or 0.8 wt % if the tungsten was initially embedded to a depth of 1 mm. The latter concentration is best supported by data in Figure 9.

If the implantation of tungsten into the alluvium is a filtration process of the kind described above, and tungsten concentrations are proportional to filtration rate and pressure, an exponentially decaying concentration profile with depth into the alluvium should be observed. This exponential concentration profile is in fact generally obeyed by data from Figure 9 plotted as individual sample points in Figure 12 (noting data scatter caused by intrinsic sampling and analysis error). The method used to fit concentration data to exponential curves is based on the assumption that the filtration mechanism can be mathematically modeled as a diffusive process, driven by a concentration gradient with a constant diffusion coefficient *D*. With this approach, the results of our tungsten analyses should provide constraints on the magnitude of filtration. Consider a one-dimensional, non-steady-state, thin-source diffusion mechanism in which the source has a concentration C_0 between 0.8 and 1.6 wt % as discussed in the preceding paragraph. The spatially and temporally varying diffusive concentrations $C(x,t)$ are given by a solution to Fourier's rate equation:

$$C(x,t) = C_0 \exp\left[\frac{-x^2}{4Dt}\right], \tag{4}$$

where x is the depth, and t is the elapsed time. This equation shows an exponentially decaying concentration profile with depth into the alluvium. We recognize that the major limitation of this equation is the assumption of constant *D*. In fact, diffusion coefficients are generally sensitive to pressure and temperature through an Arrhenius relationship,

$$D = D_0 \exp\left[\frac{-E}{RT}\right] \quad \text{for temperature, and} \tag{5}$$

$$D = D_0 \exp\left[\frac{-PV}{RT}\right] \quad \text{for pressure,} \tag{6}$$

where *D* is the diffusive coefficient extrapolated from its initial value D_0, to higher temperature *T*, and pressure *P*, for a given activation energy *E*, volume *V*, and universal gas constant, *R*. In the KISMET experiment (Kunkle, personal communication), the pressure fluctuated around 0.7 MPa (100 psi) for the first 0.2 s and then logarithmically decayed afterwards with a half-life of ~0.8 s, reaching near ambient conditions after about 5 s. The temperature also rapidly decayed from a maximum of ~ 800° C. For our purposes, we will consider the measured concentration profiles to be results of either a rapid short-time, high *D*, diffusive event of ~0.2 s after which *D* becomes infinitesimal, or a long-time, low *D*, diffusive event of ~5.0 s, again after which *D* becomes infinitesimal.

In order to test the diffusive character of our data for tungsten concentration, we plot concentration *vs* depth in Figure 12. The plot shows the fit of diffusive curves to the data using Equation (4). The best fit curve shows a surface concentration of 0.72 and diffusive coefficients of 3.19×10^{-4} m^2/s and 1.28×10^{-5} m^2/s for short time (t = 0.2 s) and long time (t = 5.0 s) respectively. Although the best fit, this curve does not seem to really predict finite tungsten concentrations deeper than about 0.03 m. To reflect the concentrations observed at greater depths, diffusive coefficients need to be increased to 2.00×10^{-3} m^2/s and 8.00×10^{-5} m^2/s

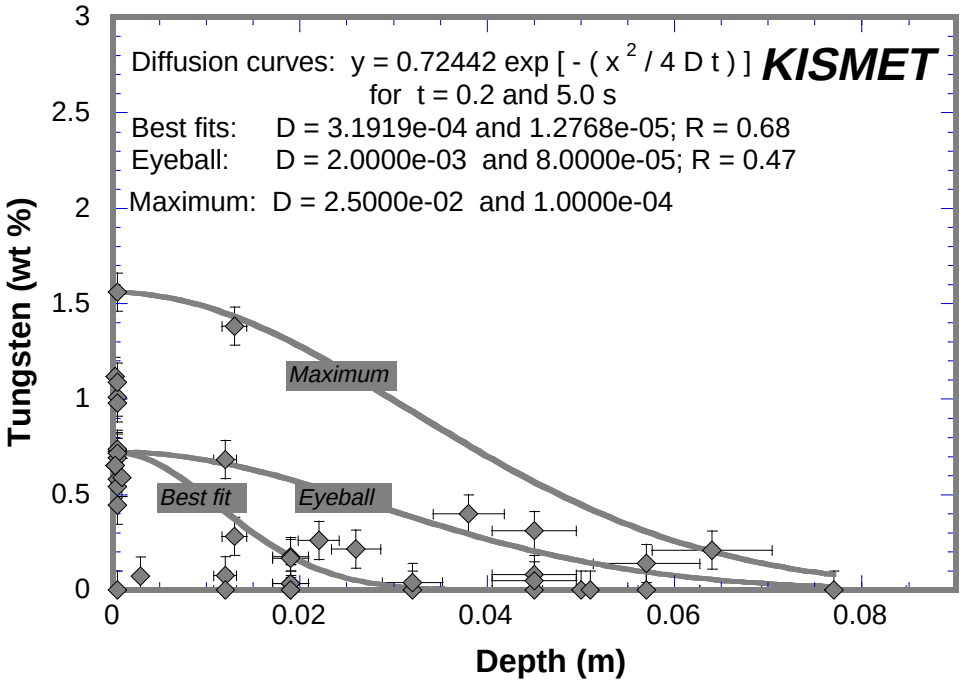

Figure 12. Tungsten concentration as a function of sample depth. Error bars are ±10% for sample depth and ±0.1 wt % for tungsten concentration. Three exponential curves are fit to the data using the diffusion model expressed in Equation (1) shown in the figure. The best fit curve shows that concentration averages ~0.72 at the surface and decays with depth with diffusion coefficients (m^2/s) for short-time (0.2 s) and long-time (5.0 s) models and a correlation coefficient of 0.68. The eyeball fit curve better approximates deeper concentrations but gives an overall poorer correlation coefficient. Lastly, a maximum fit curve brackets all concentration measurements and is most conservative for predicting the greatest penetration of tungsten into the LYNER facility alluvium.

respectively, which give perhaps more "conservative" tungsten penetration predictions with respect to environmental concerns. However, to really make a conservative prediction that provides an envelope for all data, we show a maximum diffusive curve in Figure 12, which requires diffusive coefficients of 2.50×10^{-2} m^2/s and 1.00×10^{-4} m^2/s for the short- and long-time diffusive conditions respectively.

Figure 9 shows some anomalously high average tungsten concentrations at depth. Considering a purely diffusive mechanism in a homogeneous material, there should be a smooth decrease with depth. Whether or not this observation has any statistical validity is difficult to say because of the heterogeneous nature of the tungsten implantation observed and analyses limited by the very fine size of the tungsten particles. Considering that there is some evidence that tungsten preferentially accumulated in alluvium of higher average grain size and assuming the general pore size in the alluvium increases with grain size, then if the tungsten emplacement is best described as a filtration process, more tungsten should be able to penetrate where pore spaces are larger. Following this logic, since the alluvium does contain microfractures and variations in grain sizes, then anomalously high concentrations observed at depth might be

explained by tungsten penetration along microfractures and/or pathways of higher pore space. Although our observations are certainly limited in number, the effect of rock properties and fractures likely plays an important role in determining the maximum depth of contaminant migration in any test, a feature well-learned from mine-back operations over the years at the Nevada Test Site (Carothers et al., 1995).

V. CONCLUSIONS

Tungsten used as an analog for plutonium in the KISMET experiment was dispersed by the blast and penetrated the alluvium rock forming the ribs, face, and back of the test room. Analyses of the concentrations of tungsten in the alluvium show its maximum penetration to a depth of ~0.08 m. The surface concentration of tungsten measured in samples representing the outer 1 mm of the alluvium shows a high value of ~1.5 wt %, but averaging ~0.7 wt % for all surface samples. This result supports the hypothesis that initially all of tungsten was uniformly distributed in the outer 0.5 mm of alluvium and later filtered to a maximum depth of ~80 mm. The distribution of measured tungsten concentrations in the alluvium supports a model that the emplacement mechanism (whether it is a filtration process or not) is mathematically diffusive. Maximum diffusive coefficients are 2.5×10^{-2} m^2/s and 1.0×10^{4} m^2/s for the high-pressure phase ($t = 0.2$ s) and low-pressure phase of the experiment respectively. From this diffusive model, prediction of contaminant penetration for larger explosive experiments (higher P and T) can be achieved by applying this diffusive model and scaling the diffusive coefficients by P and T through a simple Arrhenius relationship.

REFERENCES

Adushkin, V. V. and Spivak, A. A., 1994, "Geologic characterization and mechanics of underground nuclear explosions," Defense Nuclear Agency Tech. Rep. (Contract No. DNA 001-93-C-0026), Alexandria, VA.

Allen, B. M., 1995a, "Preliminary geologic site characterization of the LYNER horizontal drift complex, Yucca Flat, Nevada Test Site," Raytheon Services Nevada, TSP:DGP:080:95.

Allen, B. M., 1995b, "KISMET reentry sampling," Raytheon Services Nevada, RSN File No. 7100.2, Corres. No. TSP:DGP:078:95.

Broxton, D. E., Warren, R. G., Byers, F. M., Jr., and Scott, R. B., 1989, "Chemical and mineralogic trends within the Timber-Mountain-Oasis Valley caldera complex, Nevada: Evidence for multiple cycles of chemical evolution in a long-lived silica magma system," *J. Geophys. Res.*, V. 94, No. B5, pp. 5961-5985.

Carothers, J., et al., 1995, "Caging the dragon, the containment of underground nuclear explosions," Department of Energy (DOE/NV) Tech. Rep. 881001-951231, Las Vegas, Nevada.

Kunkle, T. D., 1994, “Containment information for LYNER KISMET,” Los Alamos National Laboratory report EES/CEP:94-014, September, 1994.

Warren, R. G., Sawyer, D. A., and Byers, Jr., F. M., 1996, Personal Communication, Los Alamos National Laboratory.

Los Alamos
NATIONAL LABORATORY
Los Alamos, New Mexico 87545